Contents lists available at ScienceDirect

Arthroplasty Today

Original research

Dual-taper modular hip implant: Investigation of 3-dimensional surface scans for component contact, shape, and fit

Nicholas B. Frisch, MD, MBA [a, *], Jonathan R. Lynch, MD [b], Robin Pourzal, PhD [c], Richard F. Banglmaier, PhD [b], Craig D. Silverton, DO [b]

[a] *Ascension Crittenton Hospital, Rochester, MI, USA*
[b] *Henry Ford Health System Department of Orthopaedic Surgery, Detroit, MI, USA*
[c] *Rush University Medical Center, Department of Orthopaedic Surgery, Chicago, IL, USA*

ARTICLE INFO

ABSTRACT

Background: The etiology of wear particle generation and subsequent corrosion in modular total hip arthroplasty implants likely begins with mechanical fretting. The purpose of this study was to determine geometric features of the male and female taper surfaces that drive stability within the neck-stem junction.
Methods: Eighteen modular hip components received 3-dimensional surface scans to examine the neck-stem taper junction using an optical scanner. The normal distance between the surfaces of the neck taper as seated in the stem slot was measured and produced a color map of the contact proximity. Contour plots identified surface shape variation and contact. Angle measurements and neck seated depth were analyzed by regression.
Results: The typical features observed were (1) a vertical line of contact at one end of the transition from the flat surface to the radius surface; (2) a vertical line of contact in the radius surface just past the centerline; (3) a concavity along the flat surface between the neck and stem components; and (4) one of the neck flat surfaces was closer to its mating surface on the stem. The seated depth of the neck was dependent on the taper angles in the flat section of the neck ($R^2 = 0.5000$, $P = .0332$).
Conclusions: The shape of the neck and stem tapers deviate from ideal design dimensions, contributing to relative motions between the neck and stem. While these processes are not proven to directly cause implant failure, they may place the implants at higher risk for failure.
© 2018 The Authors. Published by Elsevier Inc. on behalf of The American Association of Hip and Knee Surgeons. This is an open access article under the CC BY-NC-ND license (http://creativecommons.org/licenses/by-nc-nd/4.0/).

Introduction

While modularity offers increased versatility for total hip arthroplasty, corrosion of the modular junction remains an area of concern [1]. Goldberg and Gilbert were the first to describe the process of corrosion as being initiated by a mechanical mechanism in which the protective oxide layer coating the metal is disrupted; a process coined mechanically assisted crevice corrosion (MACC). Dissolution and repassivation of the oxide layer on the metal alloy ultimately leads to release of metal debris into the surrounding periprosthetic tissues, which can have countless deleterious effects [2,3]. Specifically, for Ti6Al4V/Ti6Al4V neck-stem tapers, it was shown that another material degradation process known as stress corrosion cracking can occur because of the in vivo formation of oxides within cavities [4]. A multitude of implant-related factors influence the phenomenon of these corrosion processes, including taper geometry, taper tolerances, surface finish, flexural rigidity, material composition, alloy microstructure, and number of metal-on-metal (MoM) interfaces [1].

While corrosion at the head-neck junction continues to be an area of investigation and research, corrosion has been a particular concern at the neck-stem interface of dual-taper modular implants [5-8]. Of the many implant-related factors associated with

corrosion, taper geometry and taper tolerance were 2 areas of particular interest in this report. An imperfection in the mating of components or too large a taper tolerance could potentially lead to micromotion at the taper junction and subsequent fretting corrosion with cyclic loading. The purpose of this study was to determine geometric features of the male and female taper surfaces that drive stability within the neck-stem junction. Therefore, a series of 3-dimensional (3D) surface scans on 9 pairs of newly manufactured dual-taper junctions was conducted. Our hypothesis was that implant manufacturing may not produce a uniform taper surface and that surface inconsistency will affect overall taper fit.

Material and methods

Eighteen new modular (9 stems and 9 necks) Ti6AlV4/Ti6AlV4 dual-taper modular hip implants (Profemur Z: Wright Medical Technologies, Arlington, TN) received 3D surface scans to examine the neck-stem taper junction. Before scanning, the surface of each component was coated with a thin layer of titanium dioxide powder ($\leq$10 microns) dissolved in an alcohol solvent and applied with an airbrush. Surface coating eliminates reflection and glare on polished surfaces during scanning. Reflective markers were placed on each component for spatial tracking during the digital component assembly. After paint and marker application, components were placed in a vice on a turntable and manually rotated to acquire a sequence of images producing a 3D digital reconstruction of the component. After both components were individually scanned, they were hand assembled and rescanned as an assembled modular taper. [9]

Three-dimensional scans were performed using an ATOS III Triple Scan blue light optical scanner (GOM mbH, Braunschweig, Germany) and analyzed using the GOM Inspect software application (GOM mbH, Braunschweig, Germany). The scanning system consisted of two, 8,000,000 pixel cameras. The implant image volume was resolved to a point spacing of 0.5 mm. Digitized component surface data were imported into the GOM Inspect software application, and a surface mesh of each component was created. Surface marker positions were digitally identified and used to align the individual components in the assembled positions. Surface measurement and analysis were conducted using the GOM Inspect software. Measurements were made to determine the normal distance between the surfaces of the neck taper as seated in the stem slot. These measurements were used to produce a color map of the contact proximity between the neck and stem surfaces (Fig. 1). Circumferential surface points from the neck and stem slot at corresponding taper axis heights (1.0, 3.5, 6.0, 8.5, 11.0, and 13.5 mm relative to a plane at the base of the neck) were used to create surface contour plots to identify surface shape variation and contact (Fig. 2). Taper angles for the neck and stem were determined in the straight and radius sections to compare taper shape (Fig. 3) (Table 1). Finally, the neck seated depth in the stem slot was measured.

The angle measurements and neck seated depth were analyzed by regression to identify relationships between these measurements and the implant stability, which was previously determined by the distraction force. The color map and contour plots provided a qualitative assessment of the surface shape and contact while shape tolerance deviation could not be determined without component computer-aided design data.

Results

Surface data were used to produce contact color maps. The color map was projected onto the neck component and shows the normal distance from the neck surface to the stem surface (Fig. 4).

In these contact maps were the following: (1) a distinct vertically running line of contact at one end of the transition from the flat surface section to the radius surface section, which was present on opposite surfaces in the same location; (2) a distinct vertically running line of contact in the radius surface section just past the centerline on the side further away from the transition contact and was also present on the opposite radius section in the same location; (3) a concavity or area of no contact along the flat surface exists between the neck and stem components; and (4) one of the neck flat surfaces was closer to its mating surface on the stem. The plot colors show contact proximity ranging from 0 to 0.025 mm (green), 0.025 to 0.050 mm (yellow), and 0.050 to 0.075 mm (red).

Circumferential points from the neck and stem at corresponding taper axis heights were projected onto a plane to produce surface contour plots. These plots were made to identify surface variations that explain the corresponding contact color map. The contour plot in Figure 5 shows the neck and stem surface proximity corresponding to the upper left image of the flat surface region (Fig. 4a), above. Observed is the departure of the neck and stem contour lines from left to right. This corresponds with the left to right change in color from green to yellow, illustrating a malformed neck flat section that is not truly flat. If purely dependent on position, such as an axial rotation of the neck with respect to the stem (Fig. 5, inset), the subsequent contact in the curved section would not occur at the location shown by the arrow. The contour plot shows instead a flattened variation of the neck radius, rather than a circular arc, and corresponds with the contact color map.

Mean neck taper angles in the flat (4.09°; standard deviation [SD] 0.304°) and curved (4.087°; SD 0.215°) sections were both larger than the corresponding stem taper angles in the flat (3.974°; SD 0.007°) and curved (3.967°; SD 0.020°) sections. However, neck angle in neither the flat ($P = .0882$) nor curved ($P = .0873$) section was significantly larger. Looking at the actual fit of the mating components, we observed that the neck angle variation resulted in cases where the neck taper angles were less than their mating stem taper angle. In these cases, the neck sat deeper in the stem (Fig. 6) but not significantly deeper ($P = .1034$). The average neck seated depth in the stem was 14.181 mm, ranging from 13.769 to 14.422 mm.

To determine if the difference in taper angles (S < N or S > N) influenced the seated depth of the neck, we performed a regression analysis, which showed that the seated depth of the neck was dependent on the taper angles in the flat section of the neck ($R^2 = 0.5000$, $P = .0332$). Seated depth indeed decreased as the neck taper angle increased above that of the stem taper angle.
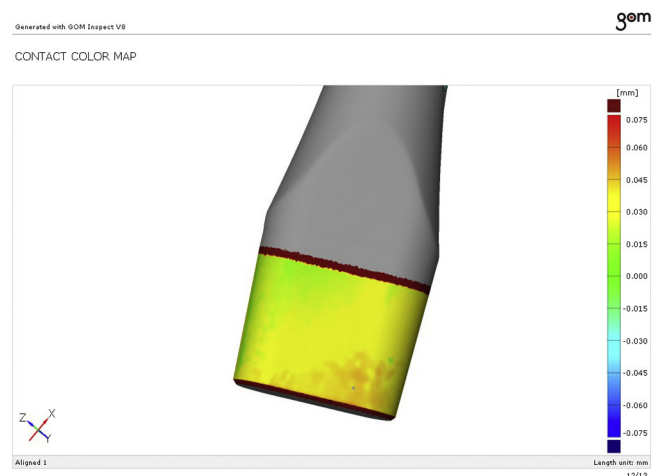
Figure 1. Representative contact color map depicting the distance between the neck and stem surfaces, which is shown on the surface of the neck.
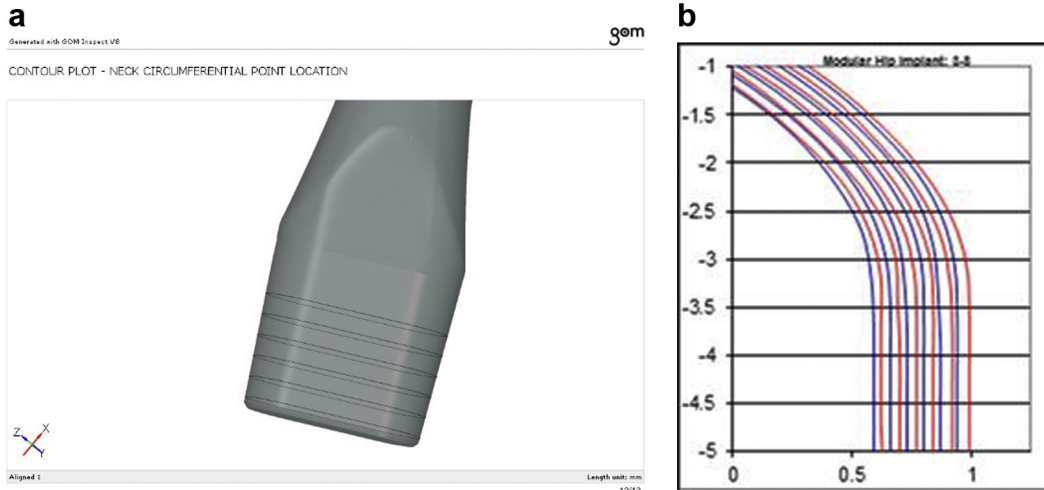
Figure 2. Circumferential lines (a) represent the location of points on the neck surface used to generate the surface contour plots (b), which were projected onto a plane at the base of the neck. The contour lines were projected onto this plane from an axial height of 1.0, 3.5, 6.0, 8.5, 11.0, and 13.5 mm. Corresponding circumferential lines on the stem slot were also projected onto this plane. Blue lines represent the neck contour, and red lines represent the stem slot contour (b).

Discussion

It was the purpose of this study to determine geometric features of the male and female taper surfaces that drive stability within the neck-stem junctions of total hip replacements with dual modular junctions. Dual-taper modularity in total hip arthroplasty allows the surgeon the capability to more precisely reconstruct hip rotation by facilitating appropriate adjustments in leg length, version, and offset [10]. This advantage comes at the expense of an additional modular MoM interface with the potential of crevice corrosion. Some studies have shown that corrosion at the modular interface is capable of generating metal ion levels that supersede that generated at the MoM articular interface [11]. Although many patients who have received such implants have experienced adverse local tissue reaction (ALTR) secondary to corrosion debris generated at the neck-stem junction [12-17], ALTR has also been observed in the absence of metallosis [18]. Fretting and corrosion can result in the generation of soluble debris that can migrate

locally or systemically and contribute to periprosthetic osteolysis, ALTR, neck fracture, or implant failure [8,19,20].

MACC is a process initiated by disruption of the protective oxide layer coating the metal by mechanical insult at the time of impaction or with cyclic loading and micromotion at the taper, the extent of which is partially determined by taper tolerance and geometry [21,22]. The diameters, angles, and tolerances of tapers are such that a small gap may exist between the tapered surfaces [22]. Such a gap, or crevice, at the taper may be large enough to allow fluid to ingress and remain stagnant while also allowing for fine-scaled, reciprocal micromotion. Micromotion promotes corrosion and fretting [23], and dual-taper implants are subjected to axial and cantilever forces which generates MoM micromotion [24]. Thus, taper geometry may play an important role in explaining the generator of corrosion at the neck-stem modular taper.

While MACC likely plays a critical role in this process, the progression of corrosion and ultimate failure of the implants is complex. Perhaps equally important and concerning is the concept of
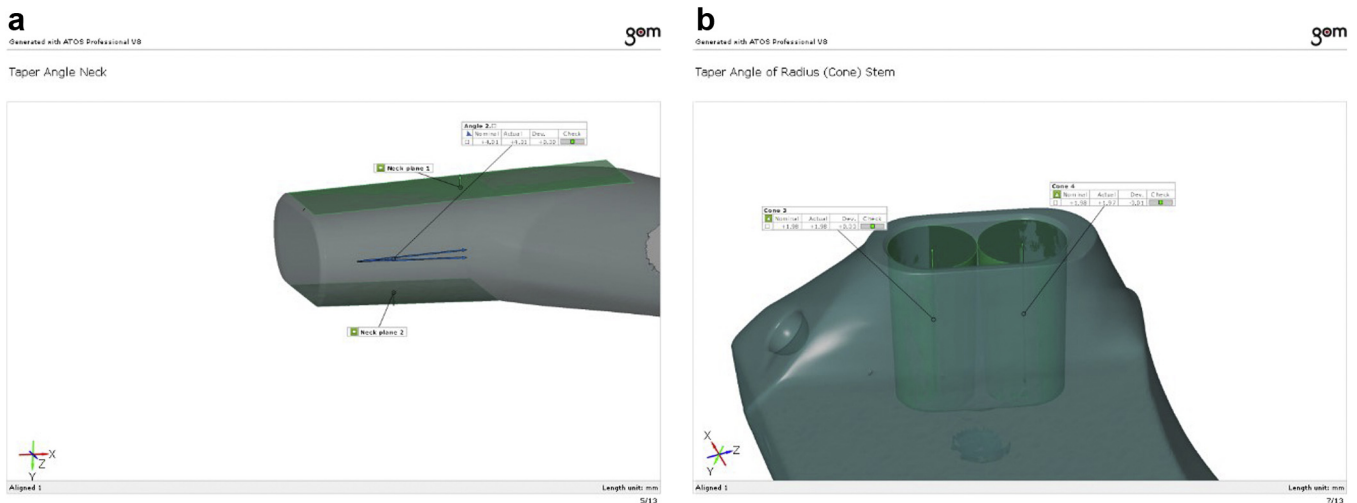
Figure 3. Taper angles from the neck and stem in the straight (a) and radius (b) sections were determined from the angle between fitted planes and cones, respectively. Not shown is the neck radius and stem straight section angles.

Table 1
Stem and neck taper angle measurements.

Taper angle	Flat stem	Flat neck	Radius stem	Radius neck
Mean	3.974	4.090	3.967	4.087
Standard deviation	0.007	0.305	0.020	0.215

The angles were measured in the straight and curved sections of the tapers. There is an angle for each straight (flat) and curved (radius) section, and there is a slight variation. However, the composite of both angles is used when describing a taper. That is to say there is an angle that each surface makes relative to the taper axis, and these 2 angles are added to describe the actual taper angle. Therefore, there will be one taper angle reported for the neck and one for the stem in the straight (flat) and curved (curved) sections.

oxide-induced stress corrosion cracking secondary to hydrogen embrittlement and tensile stress development [4]. The surface scans in this study clearly illustrate that there are specific areas of taper contact. Disruption of the oxidation layer around these areas whether during assembly or in vivo initiates the process which then progresses to autocatalytic corrosion and ultimate implant failure. Gilbert et al detailed the concept of oxide-induced stress corrosion cracking of the same implant tested in our study. They noted severe corrosion-induced damage along the medial aspect of the male taper. Our finding of a consistent vertical contact point along the radius of curvature of the male neck-stem taper suggests a possible mechanism for initiation of this process.

Taper geometric parameters such as length, taper contact area, and resultant lever arm are all factors capable of contributing to the process of corrosion [10]. The purpose of conducting a 3D surface scan investigation of the mating surfaces between the neck and stem was to identify geometric features that may contribute to corrosion processes. While the 3D scans do not tell us the extent to which the components deviate from their intended design geometries, they do provide information on the contact between the mating surfaces, the shape of the mating surfaces, and the fit of the components. Contact color maps provide a clear indication that the surfaces are not in contact over the entire circumference. In fact, they are typically in contact at 4 localized lines of contact, with some implants showing one surface in contact or closer proximity than the contralateral surface. The lines of contact run parallel to the taper axis and are symmetrically located at the end of the flat surface section, where the surface transitions into the radius surface section. The other area of contact lies in the curved surface section. These 2 contacts are similarly positioned on the opposite end to make up the 4 contact locations. Contacts located at the ends of the neck and stem may provide a pivot axis in line with the long axis of the oblong taper geometry. Such areas of contact appreciated on color maps provide potential areas of impingement during impaction, indicating a potential inciting source for corrosion. Contact color maps showing one side in contact and a gap on the other side illustrate the potential for micromotion of the taper as
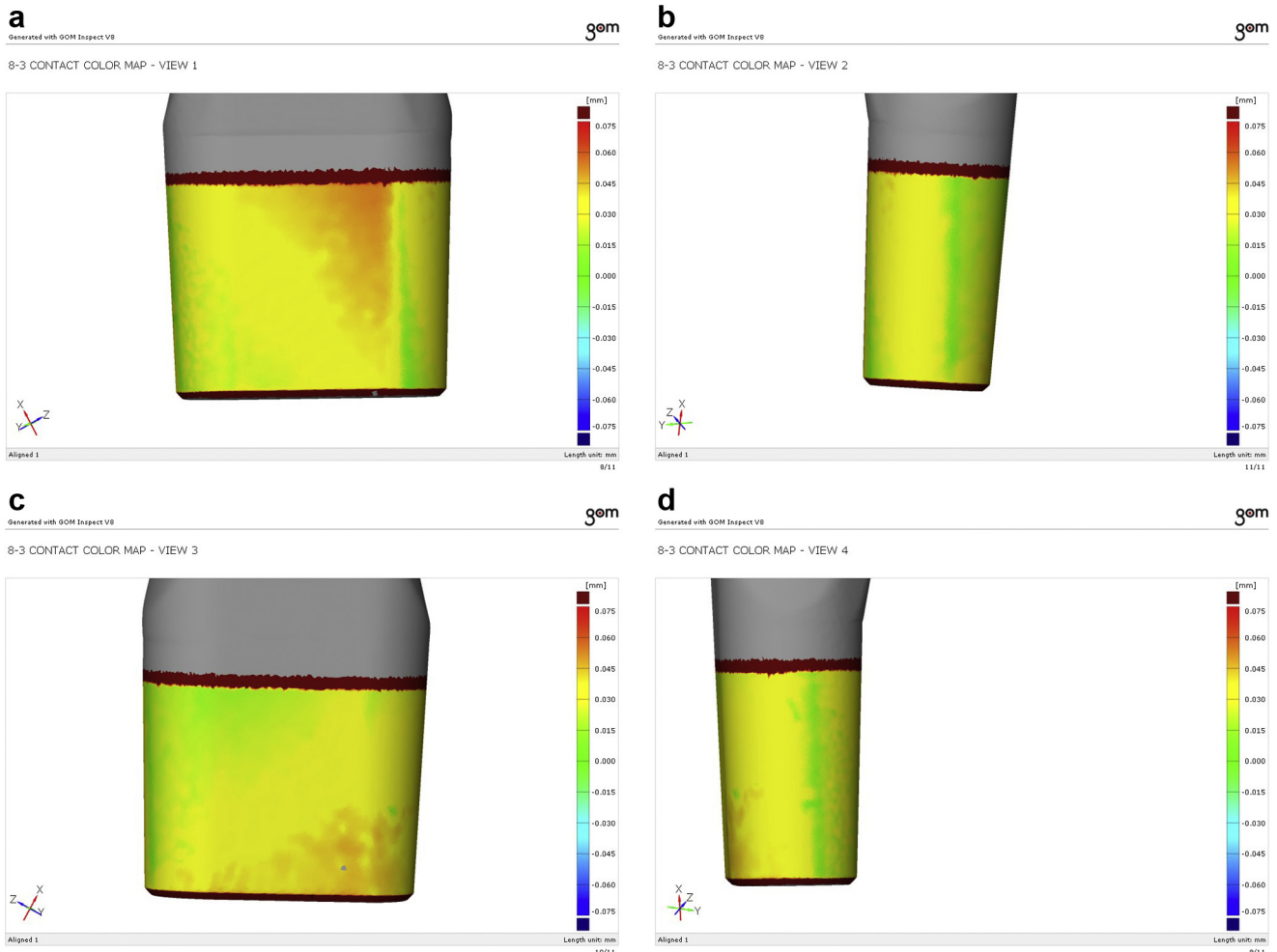
Figure 4. Contact color maps of the same implant. Image sequence (a-d) provides a 360° view of the implant and illustrates the 4 typical features.
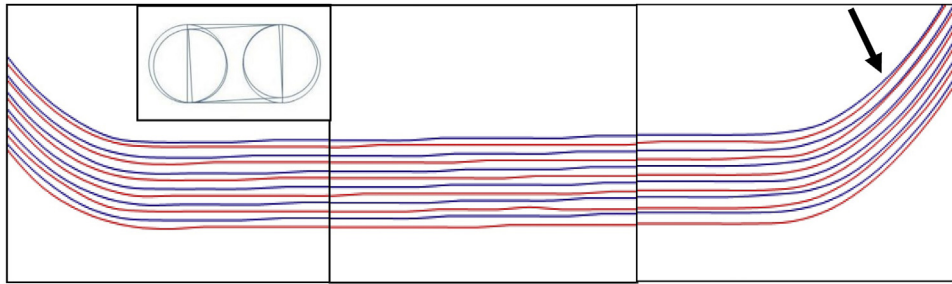
Figure 5. Contour plots of the neck and stem depicted in Figure 4a (upper left image) of the implant shown in the contact color maps, above (blue is the neck surface; red is the stem surface). The height of the rings (contour lines) increases from the inner rings to the outer rings (innermost = 1.0 mm and outermost = 13.5 mm). Note the surface variations and the departure of the neck and stem contour lines from left to right, which corresponds to the left to right change of color, from green to yellow, in the 3D contact color map. Inset depicts a neck with axial rotation relative to the stem, an ideal contact pattern that may explain the neck-stem departure along the flat surface, but does not explain the contact in the radius (arrow).

theoretically the gap between the mating surfaces should allow adequate room for the neck to rock back and forth about that pivot axis of the stem taper.

Projected contour plots of circumferential lines at different taper axis heights provide insight into the shape of the mating taper surfaces. Three key shape features were found to correspond to the contacts in the color maps. The first feature was a general closer proximity of the neck to the stem at the transition from the curved section to the flat portion of the taper followed by a gap at the taper as one moves circumferentially toward the other curved section. This pattern then repeats itself as one circumferentially returns to the starting point on the color map. Such a feature suggests that the neck is sitting in a toggled position in the stem, and these findings correlate to the colored vertical striations which are appreciated on the 3D color maps. The second feature appreciated was a closer proximity of the color plots to one another when moving from a proximal to distal direction in the axis height measured. Stated differently, there tended to be a departure of the neck from the stem as one moves more proximally in the taper contact area. Finally, there was an apparent flattening of the radius section roundness in the stem. In the contour plots, the stem surface tended to flare away from the neck surface and have a tighter curvature before flattening out and then repeating, which caused an increased gap and then contact at the transition from the flat region to the radius region, followed by the second contact after the radius centerline. Departure of the neck surface from the stem indicates a possible out-of-parallel manufacturing artifact or a tilted fit of the taper. The "toggled" fit and stem radius curvature observations may also be a manufacturing artifact. Machining marks were observed

as a striated circumferential pattern on both the neck and stem surfaces. With milling operations, there is opportunity for tool deflection due to the cutting forces arising from the cutting direction, tool speed, and feed rate [25]. The contour deviations observed in the surface scans may be explained by the changing cutting forces as the tool changes direction during the cut. However, cut deviation on the order of hundredths of a millimeter, as seen in this investigation, is not extreme [25].

Effects of shape on the neck fit in the stem is quantified by the angle and gap dimensions. The neck taper angles were typically greater than the stem taper angles, with a minority that were less than the stem taper angle. The difference in the taper angles between the neck and stem determines whether the area of contact will be more proximal (S < N) or distal (S > N) in the taper junction. Stated differently, the neck tended to seat deeper in the stem when the angle of the stem was greater than that of the neck (S > N). The gap between the neck and stem surfaces were derived from the contact maps and ranged from 0 to 0.075 mm. Whether the difference in angle and gap distance was within the taper tolerance of the design is unable to be ascertained as we were unable to get this information for the manufacturer. Nonetheless, the combination of gaps and angle difference could once again enable neck micromotion by rocking within the stem.

No prior study had been undertaken to assess surface geometry. As a result, we had no prior knowledge of the measurement variation. We agree that this was a small sample size, so we conducted a post hoc power analysis and determined that our sample size should be 17. While this would have been cost prohibitive to conduct, we feel the results are still meaningful because we anticipate that the manufacturing process is well controlled, and no previous assessment has been conducted, which attempts to investigate the taper geometry that may lead to MACC. We acknowledge that the coating process may have minimally affected the surface proximity but would not have affected the surface contour, specifically the distinct vertical contact lines. In addition, it should be noted that these components were assembled by hand. We further acknowledge that the methodology of component assembly could affect the surface proximity results but again would not affect the surface contour. There have been a variety studies comparing component assembly and suggest that variation can exist based on hand vs mallet assembly, force of impaction, and direction of impaction [9,26-28]. For the purpose of this study, hand assembly was used, but we believe that further study could be warranted to compare different assembly methods.

Conclusions

The 3D scans and analyses suggest that the shape of the neck and stem tapers deviate from ideal design dimensions, which results in a
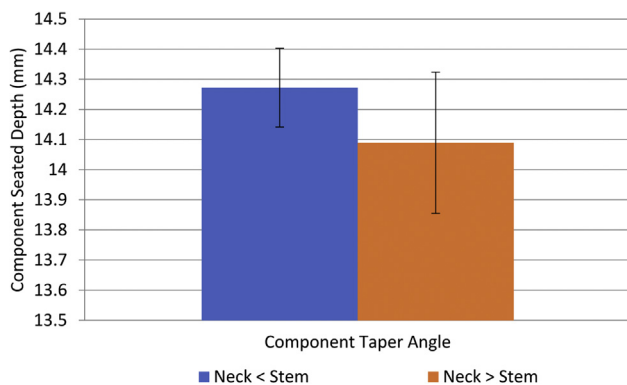
Figure 6. Neck seated depth comparison. The depth at which the neck component fit into the stem was influenced by the angle of the taper. When the neck taper angle was less than the stem taper angle the neck sat deeper in the stem than when the neck taper angle was greater than the stem taper angle.

contact pattern and component fit with gaps between the mating surfaces. The most probable cause of the dimensional deviation is due to machine tool deflection during machining. The combination of the contact and fit may contribute to relative motion between the neck and stem. While these processes are not proven to directly cause implant failure, they may place the implants at higher risk for failure.

References

[1] Jacobs JJ. Corrosion at the head-neck junction: why is this happening now? J Arthroplasty 2016;31(7):1378.
[2] Gilbert JL, Mehta M, Pinder B. Fretting crevice corrosion of stainless steel stem-CoCr femoral head connections: comparisons of materials, initial moisture, and offset length. J Biomed Mater Res B Appl Biomater 2009;88:162.
[3] Goldberg JR, Buckley C, Jacobs JJ, Gilbert JL. Corrosion testing of modular hip implants. In: Marlowe DE, Parr JE, Mayor MB, editors. Modularity of Orthopedic Implants. West Conshohocken, PA: American Society of Testing Materials; 1997.
[4] Gilbert JL, Mali S, Urban RM, Silverton CD, Jacobs JJ. In vivo oxide-induced stress corrosion cracking of Ti-6Al-4V in a neck-stem modular taper: emergent behavior in a new mechanism of in vivo corrosion. J Biomed Mater Res B Appl Biomater 2012;100(2):584.
[5] De Martino I, Assini JB, Elpers ME, Wright TM, Westrich GH. Corrosion and fretting of a modular hip system: a retrieval analysis of 60 rejuvenate stems. J Arthroplasty 2015;30(8):1470.
[6] Meftah M, Haleem AM, Burn MB, Smith KM, Incavo SJ. Early corrosion-related failure of the rejuvenate modular total hip replacement. J Bone Joint Surg Am 2014;96(6):481.
[7] Molloy DO, Munir S, Jack CM, et al. Fretting and corrosion in modular-neck total hip arthroplasty femoral stems. J Bone Joint Surg Am 2014;96(6):488.
[8] Silverton CD, Jacobs JJ, Devitt JW, Cooper HJ. Midterm results of a femoral stem with a modular neck design: clinical outcomes and metal ion analysis. J Arthroplasty 2014;29(9):1768.
[9] Pallini F, Cristofolini L, Traina F, Toni A. Modular hip stems: determination of disassembly force of a neck-stem coupling. Artif Organs 2007;31(2):166.
[10] Kwon YM. Evaluation of the painful dual taper modular neck stem total hip arthroplasty: do they all require revision? J Arthroplasty 2016;31(7):1385.
[11] Langton DJ, Sidaginamale R, Lord JK, Nargol AV, Joyce TJ. Taper junction failure in large-diameter metal-on-metal bearings. Bone Joint Res 2012;1(4):56.
[12] Cooper HJ, Urban RM, Wixson RL, Meneghini RM, Jacobs JJ. Adverse local tissue reaction arising from corrosion at the femoral neck-body junction in a dual-taper stem with a cobalt-chromium modular neck. J Bone Joint Surg Am 2013;95(10):865.
[13] Gill IP, Webb J, Sloan K, Beaver RJ. Corrosion at the neck-stem junction as a cause of metal ion release and pseudotumour formation. J Bone Joint Surg Br 2012;94(7):895.
[14] Lindgren JU, Brismar BH, Wikstrom AC. Adverse reaction to metal release from a modular metal-on-polyethylene hip prosthesis. J Bone Joint Surg Br 2011;93(10):1427.
[15] Werner SD, Bono JV, Nandi S, Ward DM, Talmo CT. Adverse tissue reactions in modular exchangeable neck implants: a report of two cases. J Arthroplasty 2013;28(3):543.e13.
[16] McGrory BJ, MacKenzie J, Babikian G. A high prevalence of corrosion at the head-neck taper with contemporary Zimmer non-cemented femoral hip components. J Arthroplasty 2015;30(7):1265.
[17] Shulman RM, Zywiel MG, Gandhi R, Davey JR, Salonen DC. Trunnionosis: the latest culprit in adverse reactions to metal debris following hip arthroplasty. Skeletal Radiol 2015;44(3):433.
[18] Ebramzadeh E, Campbell P, Tan TL, Nelson SD, Sangiorgio SN. Can wear explain the histological variation around metal-on-metal total hips? Clin Orthop Relat Res 2015;473(2):487.
[19] Lee SH, Brennan FR, Jacobs JJ, Urban RM, Ragasa DR, Glant TT. Human monocyte/macrophage response to cobalt-chromium corrosion products and titanium particles in patients with total joint replacements. J Orthop Res 1997;15(1):40.
[20] Urban RM, Jacobs JJ, Gilbert JL, Galante JO. Migration of corrosion products from modular hip prostheses. Particle microanalysis and histopathological findings. J Bone Joint Surg Am 1994;76(9):1345.
[21] Brown SA, Flemming CA, Kawalec JS, et al. Fretting corrosion accelerates crevice corrosion of modular hip tapers. J Appl Biomater 1995;6(1):19.
[22] Goldberg JR, Gilbert JL. In vitro corrosion testing of modular hip tapers. J Biomed Mater Res B Appl Biomater 2003;64(2):78.
[23] Jauch SY, Huber G, Haschke H, Sellenschloh K, Morlock MM. Design parameters and the material coupling are decisive for the micromotion magnitude at the stem-neck interface of bi-modular hip implants. Med Eng Phys 2014;36(3):300.
[24] Bobyn DTM, Krygier J, Donjovne A, Brooks E. Concernf with modularity in total hip arthroplasty. Clin Orthop Relat Res 1994;298:27.
[25] Ribeiro JLS DS, Rubio JCC, Abrāo AM. Dimensional and geometric deviations induced by milling of annealed and hardened AISI H13 tool steel. Am J Mater Sci 2012;2(1):14.
[26] Frisch NB, Lynch JR, Banglmaier RF, Silverton CD. The stability of dual-taper modular hip implants: a biomechanical analysis examining the effect of impact location on component stability. Arthroplast Today 2017;3(2):119.
[27] Frisch NB, Lynch JR, Banglmaier RF, Silverton CD. The effect of impact location on force transmission to the modular junctions of dual-taper modular hip implants. J Arthroplasty 2016;31(9):2053.
[28] Rehmer A, Bishop NE, Morlock MM. Influence of assembly procedure and material combination on the strength of the taper connection at the head-neck junction of modular hip endoprostheses. Clin Biomech (Bristol, Avon) 2012;27(1):77.